Tailoring Storage Capacity and Ion Kinetics in Ti_{2}CO_{2}/Graphene Heterostructures by Functionalization of Graphene

Cem Sevik and Deniz Çakır

Phys. Rev. Applied **12**, 014001 — Published 1 July 2019

DOI: 10.1103/PhysRevApplied.12.014001

Tailoring storage capacity and ion kinetics in Ti_2CO_2/graphene heterostructures by functionalization of graphene

Cem Sevik
Department of Mechanical Engineering, Faculty of Engineering, Anadolu University, Eskisehir, TR 26555, Turkey

Deniz Çakir*
Department of Physics and Astrophysics, University of North Dakota, Grand Forks, North Dakota 58202, USA
(Dated: June 3, 2019)

Using first-principles calculations, we evaluated the electrochemical performance of heterostructures made up of Ti_2CO_2 and chemically modified graphene for Li batteries. We found that heteroatom doping and molecule intercalation have a significant impact on the storage capacity and Li migration barrier energies. While N and S doping do not improve the storage capacity, B doping together with molecule interaction make it possible to intercalate two layers of Li which stick separately to the surface of Ti_2CO_2 and B-doped graphene. The calculated diffusion barrier energies (E_{diff}), which are between 0.3 and 0.4 eV depending on Li concentration, are quite promising for fast charge/discharge rates. Besides, the predicted E_{diff} as much as 2 eV for the diffusion of the Li atom from the Ti_2CO_2 surface to the B-doped graphene surface significantly suppresses the interlayer Li migration, which diminishes the charge/discharge rates. The calculated volume and lattice parameter changes indicate that Ti_2CO_2/graphene hybrid structures exhibit cyclic stability against Li loading/unloading. Consequently, the performed first principles calculations evidently highlight the favorable effect of molecular intercalation on the capacity improvement of ion batteries.

I. INTRODUCTION

Developments in technological applications demands highly efficient and economic energy storage devices such as rechargeable Li-ion batteries (LIBs)[1, 2]. The performance of Li-ion batteries is mainly determined by the electronic, structural and mechanical properties of constituents including electrodes and electrolytes. In this respect, two-dimensional (2D) materials with unique chemical and electronic properties are emerging as effective electrode materials for the rechargeable lithium batteries with enhanced energy and power storage density to satisfy ever increasing demands of electronic devices and electrical vehicles including cars and drones[3]. Previous theoretical and experimental works suggest that loosely packed 2D sheets with a large interlayer spacing can provide enough volume between the layers to store metal ions and help to defy the structural instabilities confronted by bulk materials such as a large volume expansion during charging/discharging cycle. Silicon anodes have been shown to undergo a volume change of 300% during lithiation and delithiation, resulting in capacity fading and limited cycle life due to severe particle pulverization, unstable solid-electrolyte interphase (SEI) formation and loss of electrical contact[4]. Therefore, 2D based electrodes are free of such large volume expansions due to binding nature between the layers. In addition, 2D materials have a large surface area that can be utilized to enhance energy and power density of Li batteries[3, 5, 6]. Further enlargement of interlayer spacing obtained through intercalation of molecules between the 2D layers provides much higher accessibility to the active sites and lower diffusion barriers that are the most important for performing high-performance energy storage[7–9]. In a recent work, we found that a high lithium storage capacity and fast kinetics can be realized for $Ti_3C_2O_2$ multilayers by preintercalating organic molecules[10]. Therefore, intercalation appears as an effective structural and chemical engineering approach for improving electrochemical performance of batteries based on 2D materials.

Graphite and non-graphitic carbon are the dominant anode materials in Li-ion batteries. Graphite shows a reversible storage capacity of 372 mA hg^{-1}[2, 11]. In spite of its excellent electrical conductivity, Li adsorption ability of graphene is poor. In a previous study, we showed that MXenes/graphene heterostructures exhibit a good compromise between storage capacity and kinetics for Li battery applications[12]. In contrast to graphene, Li ions are strongly bind to oxygen terminated MXene. In addition, presence of graphene in heterostructure ensures a good electrical conductivity that is an essential requirement for the battery applications. Similarly, diffusion barrier calculations revealed the advantage of MXene/graphene heterostructures over sole MXene systems as the energy barriers are found to be significantly lower for alkaline and earth alkaline metals.[12, 13]. Previous studies have demonstrated that chemical modification is a promising way to enhance electrochemical performance of graphene sheet[14–20]. As an example, the charge/discharge capacity of N doped graphene nanosheet increases with the charge/discharge cycles. It reaches 684 mAh/g in the 501^{st} cycle, while it is only 452 mAh/g in the 100^{th} cycle, showing higher cycling stabil-

* deniz.cakir@und.edu

ity and larger specific capacity of N-doped graphene in comparison to a pristine graphene and a commercialized graphite anode. N-doped graphene layers prepared by using chemical vapor deposition technique shows a Li storage capacity as doubled as that of pristine graphene due to the presence of a large number of surface defects[19]. Similarly, N- and B-doped graphene samples produced by using a mixed gas of NH_3BCl_3 and Ar can have a high reversible Li-capacity of > 1040 mAhg^{-1} with a rate of 50 mA^{-1}, meaning a fast charging and discharging rate[20].

MXenes, new members of 2D material family, have tunable electronic and thermal properties depending on their chemical composition and functionalization[21]. Their superior electrochemical and ion intercalation ability, very high electrical conductivity and mechanical stability make them promising materials in technological applications including batteries[22–35], capacitors[36–38], hydrogen storage[39], electromagnetic interference shielding (EMI)[40], and electronic devices[41]. We prefer to combine graphene with MXene due to following reasons: (1) many of MXenes crystals exhibit excellent metallic properties that is essential for the battery applications[42, 43]; (2) MXenes exhibits very good mechanical and dynamical stability[44]; (3) depending on type of transition metal atom and surface termination, we can tune the chemical composition and structural varieties of MXenes.

In this work, we performed first-principles calculations based on density functional theory (DFT) to evaluate the performance of heterostructure formed between chemically modified graphene and Ti_2CO_2 as an alternative electrode material for LIBs. By building heterostructures from stacking of dissimilar 2D sheets (such as MXene and graphene in this work) and pillared structures through intercalation of molecules between 2D sheets, it is possible to combine the advantages and eliminate the disadvantages of the individual monolayers[5]. As a representative example, while Ti_2CO_2 contracts during ion intercalation, graphene expands. So, by combining graphene and MXene, we can defy the significant expansion or contraction of the electrode, leading to an increased battery lifetime. Similarly, in graphite, the Li^+ intercalation follows a staging mechanism, where Li ions intercalate into specific interlayers at a time instead of random distribution into available empty interlayers. This process profoundly increases interlayer spacing and volume of the storage system[45]. In this respect, pillared structures can be used as an effective strategy to minimize the change in the interlayer distances in multilayers during ion loading/unloading. In this work, we aim to minimize interlayer expansion, and hence volume expansion, accompanying ion intercalation by introducing a benzene based organic molecule within heterostructure. We considered the attachment of organic molecule to graphene plane in order to fix it. This design principle helps to avoid diffusion of molecule together with Li ions, which may obstruct the Li migration. Moreover, we are able to realize a uniform interlayer separation between MXene and B-doped graphene sheets. In addition to the molecule intercalation, heteroatoms are introduced into the graphene framework with the expectation that the surface adsorption energy of ions is changed, the ion diffusion barrier is reduced and thus the performance of the battery is enhanced. We explored the doping and intercalation effects on the adsorption, diffusion and storage capability of Li within MXene/graphene heterostructures.

II. COMPUTATIONAL METHOD

ll calculations were performed within the framework density functional-theory (DFT), as implemented in the Vienna Ab initio Simulation package (VASP) code[46, 47]. The exchange-correlation interactions were treated using the generalized gradient approximation (GGA) within the Perdew-Burke-Ernzerhof (PBE) formulation[48] . The single electron wave functions are expanded in plane waves with kinetic energy cutoff of 400 eV. For the structure optimizations, the Brillouin-zone integrations were performed using a Γ-centered regular 5×5×1 k-point mesh within the Monkhorst-Pack scheme[49]. The convergence criterion for electronic and ionic relaxations are set as 10^{-5} and 10^{-2} eV/Å, respectively. In order to minimize the periodic interaction along the z-direction the vacuum space between the layers is taken at least 15 Å. We included van der Waals (vdW) interactions using the DFT-D3 method, including Becke-Jonson damping[50].

We calculated diffusion barriers for Li atom using the climbing-image nudge elastic (CI-NEB) method as implemented in the VASP transition state tools[51, 52]. CI-NEB is an efficient method in determining the minimum energy diffusion path between two given positions. We used a 3×3 and 5×5 super cell structures with 9 images, including initial and final positions, for CI-NEB calculations. The atomic positions and energy of the images were then relaxed. The amount of charge transfer between Li atom and MXene/graphene heterostructures were determined by using the Bader charge analysis[53–55].

III. RESULTS AND DISCUSSION

A. Energetic and structural properties of pristine and doped graphene

We first studied on the structural and electronic properties of pristine and doped graphene before investigating the considered graphene/Ti_2CO_2 heterostructures. In this work, we only considered graphitic B, N and S. In other words, we replaced a certain amount of C atoms with B or N or S without creating additional carbon vacancies near the substituent atoms. However, three different bonding configurations are possible for nitrogen in graphene, namely graphitic N,

pyridinic-like N, and pyrrolic-type N. Some experiments showed that pyridinic-N and graphitic-N are dominant configurations[56]. In a recent work, it has been shown that a relatively low partial pressure of CH_4 (mixing with NH_3) can lead to the growth of dominant pyridinic N substitutions in graphene lattice. In contrast, the growth of dominant graphitic N substitutions can be realized under a higher partial pressure of CH_4[57]. This and similar works undoubtedly point out that the doping type of N into the graphene lattice is able to be tuned by adjusting experimental growth conditions. Regarding to B-doping of graphene, Kawai *et. al.* showed that controllable doping of graphene is able to be achieved in atomic precision[58]. Similarly, in a recent work, it was showed that the reaction between benzene and boron tribromide in a closed reactor at elevated temperature (800 °C) leads to the synthesis of bulk boron-doped graphitic carbon [59].

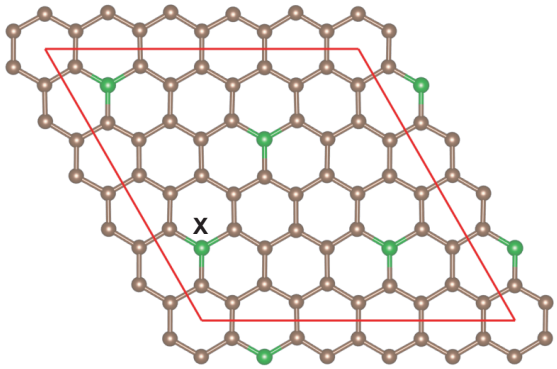

FIG. 1. Structure of a 5×5 graphene supercell used in our calculations. Green atoms (or X) are the substituent atoms.

In the 5×5 graphene supercell, as a representative example, only four carbon atoms were substituted, which corresponds to a chemical formula $C_{46}X_4$, and thus a 8% doping concentration (Fig. 1). Higher dopant concentrations increase the lattice mismatch between graphene and Ti_2CO_2. As an example, the lattice constant of pristine graphene increases from 2.46 Å to 2.59 Å when the B concentration becomes 33.3%, corresponding to a 5.2 % lattice expansion. However, for a 8% doping concentration, such expansion is only 1.25%. We selected B, N and S as substituents (or X), which have electronic configuration of $[He]2s^22p^1$, $[He]2s^22p^3$ and $[Ne]3s^23p^4$, respectively. The substituent atoms were well separated to minimize the strain effect due to size difference between C and substituent atoms. Akin to graphene, B- and N-doped graphene has almost planar structure. However, S-doped graphene exhibits a drastic deformation in the geometric structure such that each S atom forms a pyramidal like bonding configuration with three carbon atoms. To minimize induced strain within the graphene lattice, half of the S atoms appear above the graphene plane, while the other half is connected from below. Figure 2 shows the density of states of pristine and doped graphene without Li. B and N-doped systems exhibit metallic behavior, which is an essential requirement for battery applications. While B doping lowers the Fermi level down (leading to *p*-type doping), N and S rise the Fermi Level (giving rise to *n*-type doping). S doping significantly alters the electronic structure of graphene, opening a band gap with a value as much as 1 eV. A sharp peak mainly from the sulfur atoms emerges just below the Fermi level (Fig. 2(d)).

TABLE I. Binding energy of a Li ion on pristine and doped graphene in eV. @dopant (@carbon) means that Li is close to (away from) the substituent atom. The average C-C and C-substituent bond lengths are given in Å.

system	@substituent	@carbon	C-C	C-substituent
Pristine		+0.50	1.42	
B-doped	-1.12	-0.90	1.41-1.45	∼1.50
N-doped	+1.05	+0.88	1.41-1.43	∼1.41
S-doped	+0.44	+0.76	1.41-1.45	∼1.75

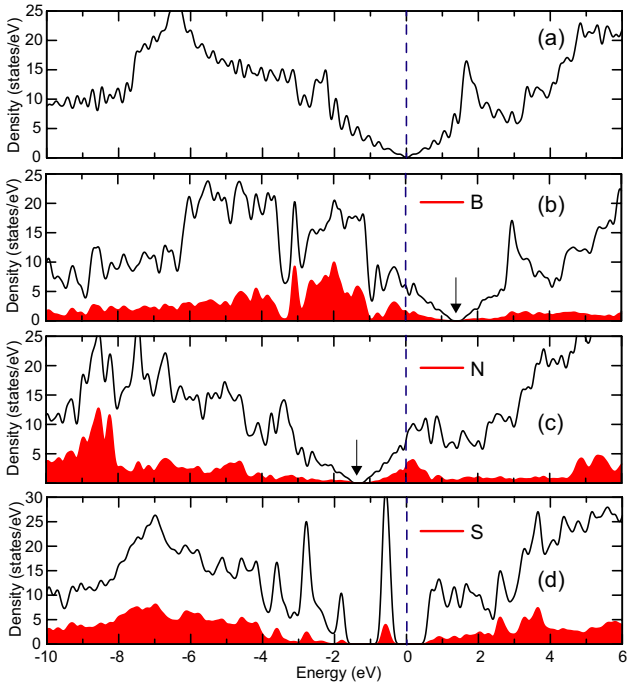

FIG. 2. Density of states (DOS) for (a) pristine, (b) B-doped, (c) N-doped and (d) S-doped graphene. The DOS for the substituent atom is represented by red color and the vertical axis is multiplied by four to make the DOS visible. The arrow marks the Dirac point in doped systems. A small band gap emerges at the Dirac point of B and N doped graphene.

To understand the influence of substituent atom on Li adsorption, the binding energy of Li on pristine and doped graphene was calculated by the formula

$$E_{bind} = E_{Tot}[C_{46}X_4 + Li] - E_{Tot}[C_{46}X_4] - \mu[Li] \quad (1)$$

where $E_{Tot}[C_{46}X_4+Li]$ and $E_{Tot}[C_{46}X_4]$ are the total energies of either pristine or doped graphene before and after introducing Li atom, and μ[Li] is the chemical potential of Li bulk. As a benchmark, we firstly computed binding energy of a single Li atom on pristine graphene (Table I). According to above definition, E_{bind} is positive, meaning that adsorption of Li on pristine graphene is an endothermic reaction, in agreement with previous studies[60, 61]. Positive E_{bind} renders graphene unsuitable for anode applications. Our findings indicate a strong effect of type of substituent atom on Li adsorption. Introducing B into graphene lattice leads to an electron deficient system. The electrons in the boron-carbon bond are shifted towards the more electronegative carbon atom. There are empty states above the valence band (Fig. 2). As Li is placed close to B-doped graphene, it tends to donate its $2s^1$ electron to this electron deficient system. Here, B-doped graphene acquires charge from Li atom, and subsequently strongly attracts positively charged Li ion, enhancing adsorption ability of graphene. The absorbed Li atom stays close to hexagon with B atom. The calculated binding energy for this adsorption structure is -1.12 eV. B-doping also affects the Li binding on C hexagons, which are well separated from B atoms, with an average binding energy of -0.90 eV. N doping results in electron rich systems, which do not tend to accept electron from Li atoms. Li binding on N-doped (S-doped) graphene is energetically less (slightly more) favorable as compared to pristine graphene. Bader charge analysis showed that the amount of charge transfer from Li to the host layer is 0.99 e in B doped graphene.

Experiments have showed an enhanced electrochemical storage performance of N-doped graphene with respect to undoped (or bare) one[18]. However, in this work, we found that graphitic N does not promise an enhanced storage performance for graphene due to unfavorable binding of Li on N-doped graphene. Our calculations revealed that p-type doping of graphene improves the adsorption of Li ion on graphene. Possible reason for experimentally observed enhanced performance in N-doped graphene can be due to the presence of C vacancies and pyridinic-N in the graphene network[62, 63]. Introducing pyridinic N atoms into graphene lattice gives rise to p-type doping, which is a suitable method to enhance the electrochemical performance of graphene. Similalry, carbon vacancy site on graphene plane was shown to serve as an attractive center for the ion, such as Li, adsorption on graphene. Computational calculations also suggested that nitrogen-decorated single and double vacancy defects in graphene appears as a promising candidate system for Li-ion batteries[64]. However, simulations for C vacancies together with pyridinic-N require much larger simulation cells to minimize the lattice mismatch with Ti_2CO_2 sheet and to ascertain the impact of isolated vacancy+pyridinic-N complex on the electrochemical properties of chemically modified graphene. Therefore, in the present study, we only considered graphitic B and N.

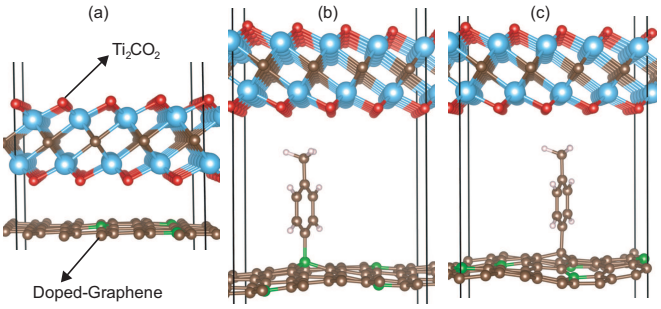

FIG. 3. A schematic representation of MXene/B-doped Graphene heterostructure (a) without and (b,c) with an intercalated molecule.

B. Energetic and structural properties of MXene/functionalized graphene heterostructures

We constructed a MXene/graphene heterostructure from a 4×4 supercell of Ti_2CO_2 and a 5×5 supercell of graphene to minimize lattice mismatch between the layers. To find out the lowest energy stacking structure, we displaced Ti_2CO_2 layer over graphene and calculated the total energy of the whole system. The interlayer separation for the ground state stacking structure is found to be around 3 Å measured between graphene and O layer of Ti_2CO_2. Then, the interface model of several structures shown in Fig. 3 were constructed to show the effect of functionalization of graphene on the Li storage capacity and kinetics. For the sake of brevity, we only scrutinized B-doped systems.

Because of the electron rich character of N and S-contained hexatomic rings, N- and S- doping are not beneficial to enhance electrochemical performances of MXene/functionalized graphene heterostructures. In a previous work, we showed that only one monolayer of Li is able to be intercalated within a Ti_2CO_2/graphene heterostructure. In order to facilitate a much better performance, we chemically doped graphene to enhance storage capacity and easy Li diffusion. In Ti_2CO_2/graphene heterostructure, we first substituted 8% of C atoms with B. The resulting structure has an interlayer separation of 2.83 Å (Fig. 3(a)). In addition to this structure, B-doped graphene was also functionalized with molecule to enlarge interlayer spacing within MXene/graphene heterostructure as shown in Fig. 3(b). Here, molecule prefers to stick to graphene sheet through a C-B bond (with a bond length of, d_{C-B}, 1.68 Å) instead of a C-C bond (d_{C-C}=1.58 Å). The former is found to be 0.70 eV energetically favorable. However, the latter structure is able to be obtained through attaching the molecule to graphene sheet prior to B doping. We also compared the stability of MXene/B-doped Gr bilayer with and without molecule by calculating the formation energies, which were obtained using the computed total energy values of MXene/B-doped Gr bilayer with/without molecule, MXene sheet, and B-doped graphene sheet with/without molecule. The formation energy was found to be 0.33

TABLE II. Binding energy of a single Li ion on MXene (@MXene) and doped graphene with molecule in eV. There are two distinct adsorption sites on doped graphene, namely @Gr-substituent and @Gr-carbon. The former (latter) means that Li is close to hexatomic ring with (without) substituent.

system	@MXene	@Gr-substituent	@Gr-carbon
B-doped MX-GR	-1.80	-1.23	-0.95
N-doped MX-GR	-1.78	+0.84	+0.60
S-doped MX-GR	-1.70	+0.52	+0.57

eV/cell or (2.3 meV/atom) for MXene/B-doped Gr bilayer with molecule, implying that the interaction between MXene and chemically modified graphene is a weak van der Waals interaction. Due to extended interlayer separation shown in Fig. 3(b) and (c), the binding energy between two monolayers is significantly small relative to MXene/B-doped graphene heterostructure without molecule denoted in Fig. 3(a) (23 meV/atom).

To asses the stability of Li adsorption within Ti_2CO_2/graphene hybrid structure, the binding energies were calculated via following expression;

$$E_{bind} = (E_{Tot}[\mathrm{MX} - \mathrm{C_{46}X_4} + n_{\mathrm{Li}}\mathrm{Li}] - E_{Tot}[\mathrm{MX} - \mathrm{C_{46}X_4}] - \mu[\mathrm{Li}])/n_{\mathrm{Li}} \quad (2)$$

where E_{Tot}[MX-$C_{46}X_4$+Li] and E_{Tot}[MX-$C_{46}X_4$] are the total energies of MXene/graphene heterostructures before and after introducing Li atom. n_{Li} is the number of Li atoms. Several possible Li adsorption sites were considered to find out the lowest energy adsorption structure of a single Li atom. It is expected that heteroatom doping can significantly change the electrochemical storage properties of graphene due to varying electronegativity difference of atoms. Regardless of structural model of heterostructure, the Li atom strongly binds to Ti_2CO_2 monolayer with an average binding energy of -1.80 eV. Expect B doped graphene, the Li atom does not stick to graphene sheet when using Li bulk chemical potential.

Figure 4 shows the variation of binding energy as a function of number of intercalated Li atoms. At first glance, the Li binding energy decreases with increasing Li concentration for the reason that repulsive interaction between Li ions makes adsorption less energetic. The rate of change of binding energy is slower for hybrid structure without molecule. In addition, B-doped graphene strengthens the interfacial Li binding by 0.3-0.5 eV in this structure (red curve in Fig. 4)

Figure 5 shows the DOS for pristine and Li intercalated Ti_2CO_2/graphene heterostructure with molecule. In pristine system, the Fermi level appears at the bottom of the conduction band of MXene layer. Occupying all available sites with Li on MXene surface, the Fermi Level moves into the conduction band of MXene (Fig. 5(b)). DOS of graphene is almost intact, meaning that there is only charge transfer between Li atoms and MXene. The calculated average Bader charge is almost +1 on Li ions,

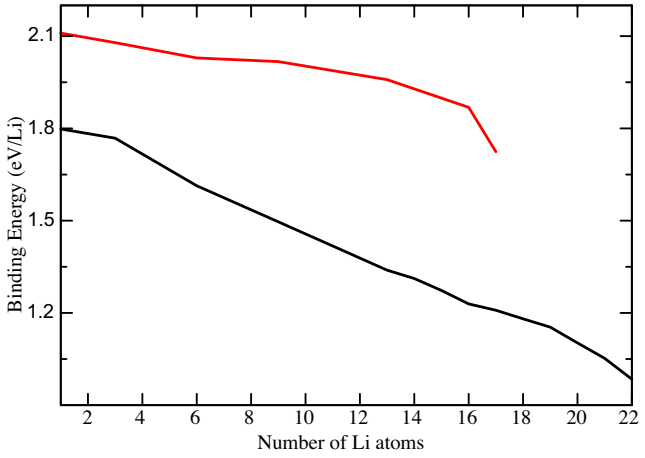

FIG. 4. Binding energy variation as a function of Li concentration. Red (black) curve denotes binding energy variation for MXene / functionalized graphene heterostructure without (with) molecule.

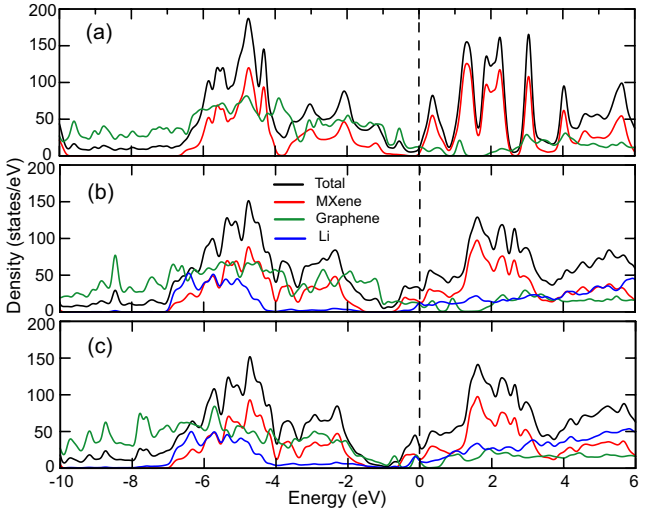

FIG. 5. PDOS of (a) pristine (b) partially and (c) fully lithiated MXene / functionalized graphene heterostructure with molecule. The vertical axis for graphene and Li is multiplied by four and twenty, respectively, to make the DOS curves visible. The Fermi level shown by black dashed line is at zero energy.

implying a complete charge transfer. Once all the active sites on MXene are occupied, the forthcoming Li ions prefer to bind to graphene sheet and concomitant charge transfer only occurs between Li and graphene (Fig. 5(c)). The calculated Bader charge is still very close to +1 for Li ions. The DOS of graphene shows about 1 eV rising of the Fermi level as a result of charge transfer.

Figure 6 shows DOS for pristine and fully lithianated Ti_2CO_2/graphene heterostructure without molecule. As is evident from Fig. 6(b), both MXene and graphene sheets accept charges from intercalated Li ions. The Fermi level moves into conduction band of MXene and

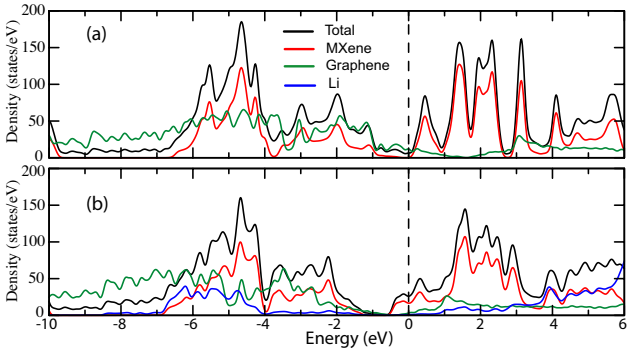

FIG. 6. PDOS of (a) pristine and (b) fully lithiated MXene / functionalized graphene heterostructure without molecule. The vertical axis for graphene and Li is multiplied by four and twenty, respectively, to make the DOS curves visible. The Fermi level shown by black dashed line is at zero energy.

graphene. The average charge on Li ions is almost +1.

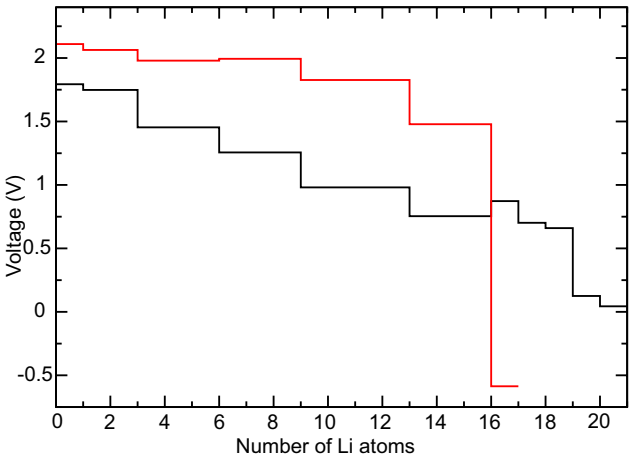

FIG. 7. Variation of average intercalation voltage as a function of Li concentration. Black (red) denotes voltage for MXene/functionalized graphene heterostructure with (without) molecule.

C. Li intercalation and average intercalation voltage

Next, the intercalation of Li atoms into MXene / functionalized graphene was investigated. Only one face of graphene and MXene were exposed to lithium adsorption to show the role of substituent atoms and molecule on the Li intercalation ability between MXene and functionalized graphene. The lithiation reaction can be written as

$$\mathrm{MX}/f\mathrm{GR}/\mathrm{Li}_x + n\mathrm{Li} \rightarrow \mathrm{MX}/f\mathrm{GR}/\mathrm{Li}_{x+n} \qquad (3)$$

where $\mathrm{MX}/f\mathrm{GR}/\mathrm{Li}_x$ denotes MXene/functionalized graphene heterostructure with x Li atoms adsorbed. Using this reaction, in order to determine the maximum storage capacity of each system, the average intercalation voltage is calculated according to following expression[32]

$$V = -\left(E_{Tot}[\mathrm{MX}/f\mathrm{GR}/\mathrm{Li}_{x+n}] - E_{Tot}[\mathrm{MX}/f\mathrm{GR}/\mathrm{Li}_x] - nE_{Tot}[\mathrm{Li}]\right)/en \qquad (4)$$

where $E_{Tot}[\mathrm{MX}/f\mathrm{GR}/\mathrm{Li}_{x+n}]$ and $E_{Tot}[\mathrm{MX}/f\mathrm{GR}/\mathrm{Li}_x]$ are the total energy of heterostructures with $x+n$ and n Li atoms, respectively. e is the absolute value of electron charge. Open circuit voltage is one of key factors which is widely calculated to characterize the performance of a battery. Before calculating V, we first searched the most stable Li adsorption configuration for each Li concentration. Figure 4 is plotted using the lowest energy adsorption configuration at each Li concentration. Owing to strong interaction of Li^+ ions with the Ti_2CO_2 surface, Li atoms first prefer to occupy all 16 active sites on MXene sheet. Then, doped-graphene starts to accept Li ions until V becomes negative at which Li clustering is energetically favorable. For MXene/functionalized graphene heterostructure with molecule (Fig. 7), the lithiation starts at voltage of around 1.79 V. This value is very close to intercalation voltage of Ti_2CO_2/pristine graphene heterostructure ($\sim$ 1.7 V), meaning that Li intercalation voltage is mainly determined by Ti_2CO_2[12]. As the 17$^{\mathrm{th}}$ atom is intercalated very close to the Li layer (which is absorbed on the surface of Ti_2CO_2), the repulsive interaction due to pre-adsorbed Li^+ ions repels this additional Li from the Ti_2CO_2 surface. However, depending on type of the substituent atom, the intercalation of the second layer is also possible. We demonstrated that the absorption of the second layer is an exothermic reaction for only B-doped graphene with molecule, whereas it is endothermic for other systems. In other words, clustering of Li atoms is energetically favorable for the latter systems. In this respect, introducing B atoms and molecule into graphene lattice significantly enhances the storage capacity. Positively charged Li ions in the second layer tend to aggregate around B atoms. Each B atom can attract only one Li atom. Interestingly, interlayer expansion without B-doping is not sufficient to realize Li adsorption on graphene. Here, the role of B-doping is to create active sites on graphene framework, which are the most important for Li storage. In our MXene/functionalized graphene heterostructure, we have chemical formula of $C_{46}B_4Li_4$ (or $C_{11.5}BLi$). B-doped graphene (with molecule) starts to determine the intercalation potential as the number of Li atoms exceeds 16. Here, we only considered one side adsorption to explore the impact of the interface formation between dissimilar materials, doping of graphene and molecule intercalation on Li storage performance and kinetics. For multilayer graphene, the maximum storage capacity is C_6Li[65]. To further increase the storage capacity, the B atom concentration should be increased. Adsorption of 17$^{\mathrm{th}}$ Li increases the lithiation voltage from 0.57 V to 0.87 V. Such an increase in voltage is attributed to an energy gain due to the adsorption of 17$^{\mathrm{th}}$ Li on B-doped

graphene. Then, subsequent addition starts to lower voltage. It drops to 0.70 V for 18^{th} Li, 0.66 V for 19^{th} Li, 0.12 V for 20^{th} and 0.04 V for 21^{th} Li atoms. When number of Li ions exceeds 21, the lithiation voltage becomes negative, meaning that Li atoms tend to form clusters rather than staying isolated. The calculated cell voltage averaged for compositions between fully lithiated and unlithiated states is 1.05 V which falls into electrochemical windows of different pertinent electrolytes[1].

Another important benefit of doping and intercalation is that the average intercalation voltage is able to be tuned by modifying heterostructure design. Enlargement of the interlayer spacing through intercalation of molecule tends to reduce intercalation potential. The calculated average voltage for MXene/functionalized graphene heterostructure without molecule is shifted upward by around 0.3-0.5 V as compared to that for MXene/functionalized graphene heterostructure with molecule. MXene/functionalized graphene heterostructure without molecule has a slower decrease rate of the intercalation potential in accordance with variation of binding energy shown in Fig. 4.

Theoretical gravimetric capacity, C (mAh/g), at maximum Li concentration (x_{max}) is computed using

$$C = \frac{x_{max} \times z \times F \times 10^3}{M_{\text{pillar}}} \tag{5}$$

where z is the valence number of Li, F is the Faraday constant (26.81 Ah/mol) and M_{pillar} is the atomic mass of pillared structure including Li atoms as well. Here, we assumed a bulk structure such that both surfaces of graphene and Ti_2CO_2 sheets accept Li ions. The calculated C is 350.3 mAh/g which is much larger than C of pristine Ti_2CO_2 (182.8 mAh/g) and Ti_2CO_2/pristine graphene heterostructure (280.5 mAh/g)[12].

D. Diffusion barriers

In addition to stability and high storage capacity, a good rate performance is required for an excellent battery application. The rate performance is controlled by electronic and ionic transport. Even though we did not calculate the electron transport properties of heterostructures, the calculated DOS plots confirm that our structures display metallic properties before and after Li adsorption. In addition, presence of lightly doped graphene ensures a good electrical conductivity in our heterostructures. We calculated the migration energy barriers (E_{diff}) along the several pathways using cNEB method. Figure 8 shows the barrier energies and corresponding pathways for the selected concentrations. At first glance, it can be seen that the calculated barrier energies are lower for MXene/functionalized graphene heterostructure as compared to commercial electrodes. At a dilute Li concentration, E_{diff} is around 0.25-0.32 eV for the on-plane Li diffusion. In contrast, we found a very large diffusion barrier energy for the out-of-plane diffusion. This means that once a Li atom is adsorbed on either MXene or graphene, it most likely stays there. We also computed E_{diff} for two different high Li concentrations. While we only have one Li vacancy in the first configuration, two nearby Li vacancies are created in the second case on the surface of Ti_2CO_2. These two configurations give rise to totally different barrier energies. Fig. 8(d) displays barrier energy profile and path for the two-vacancy structure ($x = 0.90$). Here, E_{diff} is around 0.3 eV and not much different than that of structures with a single Li atom absorbed (Fig. 8(c)). However, single vacancy structure results in an E_{diff} of 0.72 eV ($x = 0.95$). Our calculations imply two main regimes for ion transport. Up to Li content of x=0.90, E_{diff} is low. When x exceeds 0.90, E_{diff} increases substantially. This is due to a steric effect that obstructs the diffusion of Li^+ in single vacancy case (i.e $x > 0.90$). In two vacancy-case ($x < 0.90$), there is enough space for migrating Li ion to avoid nearby Li^+ ions. Interestingly, the diffusion barrier of a single Li atom between Ti_2CO_2 and B-doped graphene without molecule is around 0.30 eV which is comparable with heterostructure with molecule. This is due to that we can weaken the strong effect of geometric constraint that is present in pristine multilayers by constructing heterostructures. Table III summarizes the barrier energies for several paths with different Li concentrations.

E. Cycling stability

We determined interlayer separation, lattice parameter and volume changes during the Li intercalation/deintercalation to test cyclic stability of MXene/functionalized graphene heterostructures. First of all, we found no bond breaking. The C-B bond connecting molecule to graphene becomes 1.67 Å for fully lithiated state with a change of -1.1% as compared to unlithiated state. The in-plane lattice parameters shrink only 0.5%. Due to the enlarged lattice spacing, all active sites are easily reachable by Li ions without any need for a large interlayer expansion. The total expansion along the vertical direction is around 6.5% (measured from unexposed O layer of Ti_2CO_2 to graphene layer), which is smaller than that of graphite (10%).

IV. CONCLUSION

In this work, we demonstrated that heterostructures made up of MXene and functionalized graphene are promising candidate structures to control and manipulate the generation and diffusion of Li ions within interface of dissimilar materials. We chemically modified graphene sheet with B and molecule. While the role of molecule is to enlarge interlayer distance, B-doping is utilized to introduce active sites on graphene sheet to enhance storage capacity. B-doping significantly enhances Li binding on graphene. Molecule intercalation

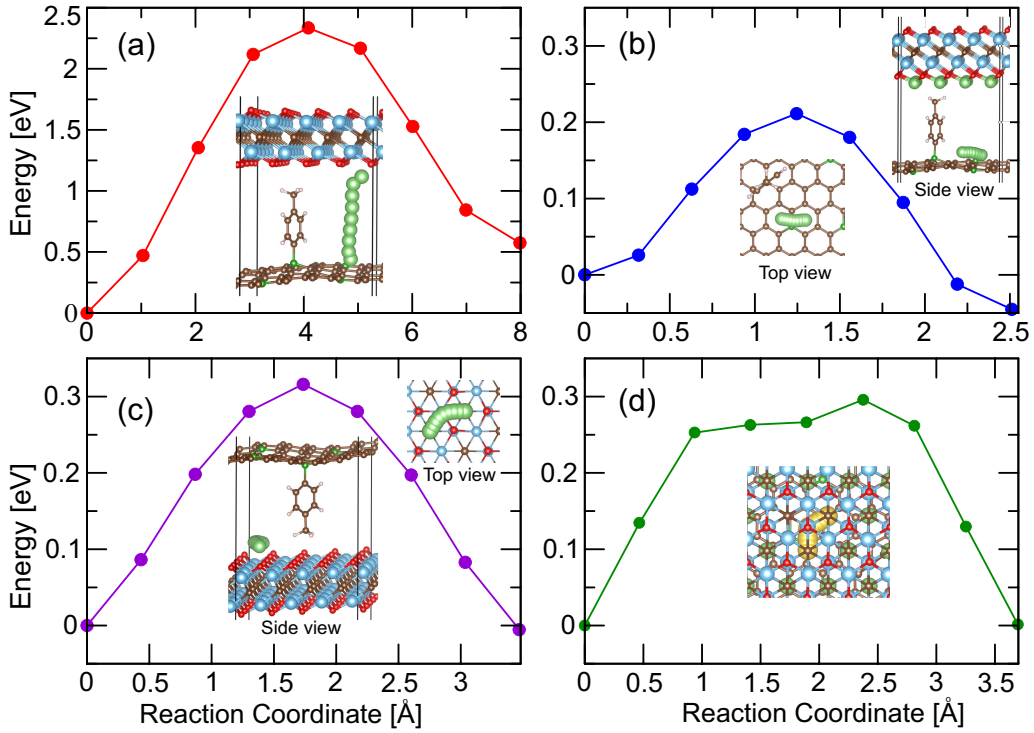

FIG. 8. The diffusion energy profiles and corresponding migration paths for the selected systems. In (d), the migrating Li atom is denoted by yellow color.

TABLE III. Calculated diffusion barriers for several migration paths in eV. Barrier-1 is the diffusion barrier of a single Li ion on MXene sheet, corresponding to x=0.05 (Fig. 8(c)). Barrier-2 (Barrier-3) denotes the diffusion barrier of a single Li ion for the concentration of x=0.88 (0.94) on MXene sheet. Fig. 8(d) shows the migration path for Barrier-2. Barrier-4 (Fig. 8(b)) is the diffusion barrier of a single Li ion on B-doped graphene for x=0.05. Finally, Barrier-5 (Fig. 8(a)) represents the diffusion of a single Li ion from MXene sheet to B-doped graphene sheet.

Barrier-1 @MXene (x=0.05)	Barrier-2 @MXene (x=0.90)	Barrier-3 @MXene (x=0.95)	Barrier-4 @Gr (x=0.05)	Barrier-5 MXene→Gr
0.32	0.30	0.72	0.21	2.33

(i.e. interlayer expansion) is mandatory to make use of B-doping for gravimetric capacity improvement. It turns out that the MXene/functionalized graphene heterostructures provide a good electrical conductivity and low diffusions barriers as evidence from band structure and migration energy calculations. We can realize diffusion barriers as low as 0.3 eV even for high Li concentrations. The out-of plane diffusions barriers are at least six times larger than in-plane diffusion barriers, thus implying that Li ions move laterally on either MXene or graphene plane. As compared to pristine MXene multilayers and MXene/functionalized graphene without molecule, an enhanced storage capacity is able to be achieved with a value of 350.3 mAh/g for MXene/functionalized graphene with molecule. Combining graphene with MXene markedly limits the volume change that is critical to eliminate restacking and maintain a cyclic stability.

V. ACKNOWLEDGEMENT

Computer resources used in this work is provided by Computational Research Center (HPC-Linux cluster) at University of North Dakota, the High Performance and Grid Computing Center (TRGrid e-Infrastructure) of TUBITAK ULAKBIM, and the National Center for High Performance Computing (UHeM) of Istanbul Technical University. A part of this work was supported by University of North Dakota Early Career Award (Grant number: 20622-4000-02624). We also acknowledge financial support from ND EPSCoR through NSF grant OIA-1355466. C. S. acknowledges the support from the TUBITAK (116F080) and the BAGEP Award of the Science Academy. This work was performed, in part, at the Center for Nanoscale Materials, a U.S. Department of Energy Office of Science User Facility, and supported by the U.S. Department of Energy, Office of Science, under

contract no. DE-AC02- 06CH11357.

[1] J. B. Goodenough and Y. Kim, Challenges for rechargeable li batteries, Chemistry of Materials **22**, 587 (2010), https://doi.org/10.1021/cm901452z.

[2] J.-M. Tarascon and M. Armand, Issues and challenges facing rechargeable lithium batteries, Nature **414**, 359 (2001).

[3] B. Anasori, M. R. Lukatskaya, and Y. Gogotsi, 2d metal carbides and nitrides (mxenes) for energy storage, Nature Reviews Materials **2**, 16098 EP (2017).

[4] Y. Jin, B. Zhu, Z. Lu, N. Liu, and J. Zhu, Challenges and recent progress in the development of si anodes for lithium-ion battery, Advanced Energy Materials **7**, 1700715 (2017), https://onlinelibrary.wiley.com/doi/pdf/10.1002/aenm.201700715.

[5] E. Pomerantseva and Y. Gogotsi, Two-dimensional heterostructures for energy storage, Nature Energy **2**, 17089 EP (2017).

[6] T. Kocabas, A. Ozden, I. Demircioglu, D. Cakir, and C. Sevik, Determination of dynamically stable electrenes toward ultrafast charging battery applications, The Journal of Physical Chemistry Letters **9**, 4267 (2018), https://doi.org/10.1021/acs.jpclett.8b01468.

[7] J. Mei, Y. Zhang, T. Liao, Z. Sun, and S. X. Dou, Strategies for improving the lithium-storage performance of 2d nanomaterials, National Science Review **5**, 389 (2018).

[8] P. Simon, Two-dimensional mxene with controlled interlayer spacing for electrochemical energy storage, ACS Nano **11**, 2393 (2017), https://doi.org/10.1021/acsnano.7b01108.

[9] J. Luo, W. Zhang, H. Yuan, C. Jin, L. Zhang, H. Huang, C. Liang, Y. Xia, J. Zhang, Y. Gan, and X. Tao, Pillared structure design of mxene with ultralarge interlayer spacing for high-performance lithium-ion capacitors, ACS Nano **11**, 2459 (2017), https://doi.org/10.1021/acsnano.6b07668.

[10] E. M. D. Siriwardane, I. Demiroglu, C. Sevik, and D. Cakir, Achieving fast kinetics and enhanced li storage capacity for ti3c2o2 by intercalation of quinone molecules, ACS Applied Energy Materials **2**, 1251 (2019), https://doi.org/10.1021/acsaem.8b01801.

[11] J. R. Dahn, T. Zheng, Y. Liu, and J. S. Xue, Mechanisms for lithium insertion in carbonaceous materials, Science **270**, 590 (1995), http://science.sciencemag.org/content/270/5236/590.full.pdf.

[12] Y. Aierken, C. Sevik, O. Gulseren, F. M. Peeters, and D. Cakir, Mxenes/graphene heterostructures for li battery applications: a first principles study, J. Mater. Chem. A **6**, 2337 (2018).

[13] I. Demiroglu, F. M. Peeters, O. Gulseren, D. Cakir, and C. Sevik, Alkali metal intercalation in mxene/graphene heterostructures: A new platform for ion battery applications, The Journal of Physical Chemistry Letters **10**, 727 (2019), https://doi.org/10.1021/acs.jpclett.8b03056.

[14] X. Wang, Q. Weng, X. Liu, X. Wang, D.-M. Tang, W. Tian, C. Zhang, W. Yi, D. Liu, Y. Bando, and D. Golberg, Atomistic origins of high rate capability and capacity of n-doped graphene for lithium storage, Nano Letters **14**, 1164 (2014), https://doi.org/10.1021/nl4038592.

[15] Y. Yang, D.-M. Tang, C. Zhang, Y. Zhang, Q. Liang, S. Chen, Q. Weng, M. Zhou, Y. Xue, J. Liu, J. Wu, Q. H. Cui, C. Lian, G. Hou, F. Yuan, Y. Bando, D. Golberg, and X. Wang, Protrusions or holes in graphene: which is the better choice for sodium ion storage?, Energy Environ. Sci. **10**, 979 (2017).

[16] L. Zhou, Z. F. Hou, B. Gao, and T. Frauenheim, Doped graphenes as anodes with large capacity for lithium-ion batteries, J. Mater. Chem. A **4**, 13407 (2016).

[17] Y. Liu, V. I. Artyukhov, M. Liu, A. R. Harutyunyan, and B. I. Yakobson, Feasibility of lithium storage on graphene and its derivatives, The Journal of Physical Chemistry Letters **4**, 1737 (2013), https://doi.org/10.1021/jz400491b.

[18] X. Li, D. Geng, Y. Zhang, X. Meng, R. Li, and X. Sun, Superior cycle stability of nitrogen-doped graphene nanosheets as anodes for lithium ion batteries, Electrochemistry Communications **13**, 822 (2011).

[19] A. L. M. Reddy, A. Srivastava, S. R. Gowda, H. Gullapalli, M. Dubey, and P. M. Ajayan, Synthesis of nitrogen-doped graphene films for lithium battery application, ACS Nano **4**, 6337 (2010), https://doi.org/10.1021/nn101926g.

[20] Z.-S. Wu, W. Ren, L. Xu, F. Li, and H.-M. Cheng, Doped graphene sheets as anode materials with superhigh rate and large capacity for lithium ion batteries, ACS Nano **5**, 5463 (2011), https://doi.org/10.1021/nn2006249.

[21] N. Michael, M. V. N., B. M. W., and G. Yury, 25th anniversary article: Mxenes: A new family of two-dimensional materials, Advanced Materials **26**, 992, https://onlinelibrary.wiley.com/doi/pdf/10.1002/adma.201304138.

[22] M. Naguib, O. Mashtalir, J. Carle, V. Presser, J. Lu, L. Hultman, Y. Gogotsi, and M. W. Barsoum, Two-dimensional transition metal carbides, ACS Nano **6**, 1322 (2012), https://doi.org/10.1021/nn204153h.

[23] Y. Sun, D. Chen, and Z. Liang, Two-dimensional mxenes for energy storage and conversion applications, Materials Today Energy **5**, 22 (2017).

[24] B. Anasori, M. R. Lukatskaya, and Y. Gogotsi, 2d metal carbides and nitrides (mxenes) for energy storage, Nature Reviews Materials **2**, 16098 (2017).

[25] C. Eames and M. S. Islam, Ion intercalation into two-dimensional transition-metal carbides: Global screening for new high-capacity battery materials, Journal of the American Chemical Society **136**, 16270 (2014), https://doi.org/10.1021/ja508154e.

[26] Y. Xie, M. Naguib, V. N. Mochalin, M. W. Barsoum, Y. Gogotsi, X. Yu, K.-W. Nam, X.-Q. Yang, A. I. Kolesnikov, and P. R. C. Kent, Role of surface structure on li-ion energy storage capacity of two-dimensional transition-metal carbides,

Journal of the American Chemical Society **136**, 6385 (2014), https://doi.org/10.1021/ja501520b.
[27] M. Naguib, J. Come, B. Dyatkin, V. Presser, P.-L. Taberna, P. Simon, M. W. Barsoum, and Y. Gogotsi, Mxene: a promising transition metal carbide anode for lithium-ion batteries, Electrochemistry Communications **16**, 61 (2012).
[28] Z. Lin, D. Sun, Q. Huang, J. Yang, M. W. Barsoum, and X. Yan, Carbon nanofiber bridged two-dimensional titanium carbide as a superior anode for lithium-ion batteries, J. Mater. Chem. A **3**, 14096 (2015).
[29] Y. Xie, Y. Dall'Agnese, M. Naguib, Y. Gogotsi, M. W. Barsoum, H. L. Zhuang, and P. R. C. Kent, Prediction and characterization of mxene nanosheet anodes for non-lithium-ion batteries, ACS Nano **8**, 9606 (2014), http://dx.doi.org/10.1021/nn503921j.
[30] A. Byeon, M.-Q. Zhao, C. E. Ren, J. Halim, S. Kota, P. Urbankowski, B. Anasori, M. W. Barsoum, and Y. Gogotsi, Two-dimensional titanium carbide mxene as a cathode material for hybrid magnesium/lithium-ion batteries, ACS Applied Materials & Interfaces **9**, 4296 (2017), https://doi.org/10.1021/acsami.6b04198.
[31] D. Er, J. Li, M. Naguib, Y. Gogotsi, and V. B. Shenoy, Ti3c2 mxene as a high capacity electrode material for metal (li, na, k, ca) ion batteries, ACS Applied Materials & Interfaces **6**, 11173 (2014), https://doi.org/10.1021/am501144q.
[32] D. Cakir, C. Sevik, O. Gulseren, and F. M. Peeters, Mo2c as a high capacity anode material: a first-principles study, J. Mater. Chem. A **4**, 6029 (2016).
[33] Q. Tang, Z. Zhou, and P. Shen, Are MXenes Promising Anode Materials for Li Ion Batteries? Computational Studies on Electronic Properties and Li Storage Capability of Ti3C2 and Ti3C2 X2 (X = F, OH) Monolayer, J. Am. Chem. Soc. **134**, 16909 (2012).
[34] S. Kajiyama, L. Szabova, K. Sodeyama, H. Iinuma, R. Morita, K. Gotoh, Y. Tateyama, M. Okubo, and A. Yamada, Sodium-ion intercalation mechanism in mxene nanosheets, ACS Nano **10**, 3334 (2016), https://doi.org/10.1021/acsnano.5b06958.
[35] C. Wang, H. Xie, S. Chen, B. Ge, D. Liu, C. Wu, W. Xu, W. Chu, G. Babu, P. M. Ajayan, and L. Song, Atomic cobalt covalently engineered interlayers for superior lithium-ion storage, Advanced Materials **30**, 1802525, https://onlinelibrary.wiley.com/doi/pdf/10.1002/adma.201802525.
[36] M. R. Lukatskaya, O. Mashtalir, C. E. Ren, Y. Dall'Agnese, P. Rozier, P. L. Taberna, M. Naguib, P. Simon, M. W. Barsoum, and Y. Gogotsi, Cation intercalation and high volumetric capacitance of two-dimensional titanium carbide, Science **341**, 1502 (2013), http://science.sciencemag.org/content/341/6153/1502.full.pdf.
[37] X. Wang, S. Kajiyama, H. Iinuma, E. Hosono, S. Oro, I. Moriguchi, M. Okubo, and A. Yamada, Pseudocapacitance of mxene nanosheets for high-power sodium-ion hybrid capacitors, Nature Communications **6**, 6544 (2015).
[38] L. Jian, Y. Xiaotao, L. Cong, Y. Yanquan, X. Le, D. Xin, X. Jinglin, L. Jianhua, and S. Junliang, Achieving high pseudocapacitance of 2d titanium carbide (mxene) by cation intercalation and surface modification, Advanced Energy Materials **7**, 1602725, https://onlinelibrary.wiley.com/doi/pdf/10.1002/aenm.201602725.
[39] Q. Hu, D. Sun, Q. Wu, H. Wang, L. Wang, B. Liu, A. Zhou, and J. He, Mxene: A new family of promising hydrogen storage medium, The Journal of Physical Chemistry A **117**, 14253 (2013), https://doi.org/10.1021/jp409585v.
[40] F. Shahzad, M. Alhabeb, C. B. Hatter, B. Anasori, S. Man Hong, C. M. Koo, and Y. Gogotsi, Electromagnetic interference shielding with 2d transition metal carbides (mxenes), Science **353**, 1137 (2016), http://science.sciencemag.org/content/353/6304/1137.full.pdf.
[41] X. Bingzhe, Z. Minshen, Z. Wencong, Z. Xu, P. Zengxia, X. Qi, Z. Chunyi, and S. Peng, Ultrathin mxene-micropattern-based field-effect transistor for probing neural activity, Advanced Materials **28**, 3333 (2016), https://onlinelibrary.wiley.com/doi/pdf/10.1002/adma.201504657.
[42] M. Khazaei, A. Ranjbar, M. Arai, T. Sasaki, and S. Yunoki, Electronic properties and applications of mxenes: a theoretical review, J. Mater. Chem. C **5**, 2488 (2017).
[43] Z. Ling, C. E. Ren, M.-Q. Zhao, J. Yang, J. M. Giammarco, J. Qiu, M. W. Barsoum, and Y. Gogotsi, Flexible and conductive mxene films and nanocomposites with high capacitance, Proceedings of the National Academy of Sciences **111**, 16676 (2014), http://www.pnas.org/content/111/47/16676.full.pdf.
[44] U. Yorulmaz, A. Ozden, N. K. Perkgoz, F. Ay, and C. Sevik, Vibrational and mechanical properties of single layer mxene structures: a first-principles investigation, Nanotechnology **27**, 335702 (2016).
[45] J. Hui, M. Burgess, J. Zhang, and J. Rodriguez-Lopez, Layer number dependence of li+ intercalation on few-layer graphene and electrochemical imaging of its solid?electrolyte interphase evolution, ACS Nano **10**, 4248 (2016), pMID: 26943950, https://doi.org/10.1021/acsnano.5b07692.
[46] G. Kresse and J. Furthmüller, Efficiency of *ab initio* total energy calculations for metals and semiconductors using a plane-wave basis set, Comput. Mater. Sci. **6**, 15 (1996).
[47] G. Kresse and J. Furthmüller, Efficient iterative schemes for *ab initio* total-energy calculations using a plane-wave basis set, Phys. Rev. B **54**, 11169 (1996).
[48] J. P. Perdew, K. Burke, and M. Ernzerhof, Generalized gradient approximation made simple, Phys. Rev. Lett. **77**, 3865 (1996).
[49] H. J. Monkhorst and J. D. Pack, Special points for brillouin-zone integrations, Phys. Rev. B **13**, 5188 (1976).
[50] G. Stefan, E. Stephan, and G. Lars, Effect of the damping function in dispersion corrected density functional theory, Journal of Computational Chemistry **32**, 1456, https://onlinelibrary.wiley.com/doi/pdf/10.1002/jcc.21759.
[51] G. Henkelman, B. P. Uberuaga, and H. Jansson, A climbing image nudged elastic band method for finding saddle points and minimum energy paths, The Journal of Chemical Physics **113**, 9901-9904 (2000).
[52] G. Henkelman and H. Jansson, Improved tangent estimate in the nudged elastic band method for finding minimum energy paths and saddle points, The Journal of Chemical Physics **113**, 9978-9985 (2000).

[53] W. Tang, E. Sanville, and G. Henkelman, A grid-based bader analysis algorithm without lattice bias, J. Phys.: Condens. Matter **21**, 084204 (2009).
[54] E. Sanville, S. D. Kenny, R. Smith, and G. Henkelman, An improved grid-based algorithm for bader charge allocation, J. Comp. Chem. **28**, 899 (2007).
[55] G. Henkelman, A. Arnaldsson, and H. Jónsson, A fast and robust algorithm for bader decomposition of charge density, Comput. Mater. Sci. **36**, 254 (2006).
[56] L. Zhao, R. He, K. T. Rim, T. Schiros, K. S. Kim, H. Zhou, C. Gutiérrez, S. P. Chockalingam, C. J. Arguello, L. Pálová, D. Nordlund, M. S. Hybertsen, D. R. Reichman, T. F. Heinz, P. Kim, A. Pinczuk, G. W. Flynn, and A. N. Pasupathy, Visualizing individual nitrogen dopants in monolayer graphene, Science **333**, 999 (2011), http://science.sciencemag.org/content/333/6045/999.full.pdf.
[57] C. Ma, Q. Liao, H. Sun, S. Lei, Y. Zheng, R. Yin, A. Zhao, Q. Li, and B. Wang, Tuning the doping types in graphene sheets by n monoelement, Nano Letters **18**, 386 (2018), https://doi.org/10.1021/acs.nanolett.7b04249.
[58] S. Kawai, S. Saito, S. Osumi, S. Yamaguchi, A. S. Foster, P. Spijker, and E. Meyer, Atomically controlled substitutional boron-doping of graphene nanoribbons, Nature Communications **6**, 8098 EP (2015).
[59] N. P. Stadie, E. Billeter, L. Piveteau, K. V. Kravchyk, M. Dobeli, and M. V. Kovalenko, Direct synthesis of bulk boron-doped graphitic carbon, Chemistry of Materials **29**, 3211 (2017), https://doi.org/10.1021/acs.chemmater.7b00376.
[60] E. Lee and K. A. Persson, Li absorption and intercalation in single layer graphene and few layer graphene by first principles, Nano Letters **12**, 4624 (2012), https://doi.org/10.1021/nl3019164.
[61] Y. Shaidu, E. Kucukbenli, and S. de Gironcoli, Lithium adsorption on graphene at finite temperature, The Journal of Physical Chemistry C **122**, 20800 (2018), https://doi.org/10.1021/acs.jpcc.8b05689.
[62] X.-k. Kong and Q.-w. Chen, Improved performance of graphene doped with pyridinic n for li-ion battery: a density functional theory model, Phys. Chem. Chem. Phys. **15**, 12982 (2013).
[63] X. Fan, W. Zheng, and J.-L. Kuo, Adsorption and diffusion of li on pristine and defective graphene, ACS Applied Materials & Interfaces **4**, 2432 (2012), https://doi.org/10.1021/am3000962.
[64] Y.-X. Yu, Can all nitrogen-doped defects improve the performance of graphene anode materials for lithium-ion batteries?, Phys. Chem. Chem. Phys. **15**, 16819 (2013).
[65] E. Hazrati, G. A. de Wijs, and G. Brocks, Li intercalation in graphite: A van der waals density-functional study, Phys. Rev. B **90**, 155448 (2014).